Spin-orbit coupling induced degeneracy in the anisotropic unconventional superconductor UTe$_2$

Alexander B. Shick ⬤

Institute of Physics, Czech Academy of Science, Na Slovance 2, CZ-18221 Prague, Czech Republic

Warren E. Pickett ⬤*

Department of Physics, University of California Davis, Davis, California 95616, USA

The orthorhombic uranium dichalcogenide UTe$_2$ displays superconductivity below 1.7 K, with the anomalous feature of retaining 50% of normal state (ungapped) carriers, according to heat capacity data from two groups. Incoherent transport that crosses over from above 50 K toward a low-temperature, Kondo lattice Fermi liquid regime indicates strong magnetic fluctuations and the need to include correlation effects in theoretical modeling. We report density functional theory plus Hubbard U (DFT+U) results for UTe$_2$ to provide a platform for modeling its unusual behavior, focusing on ferromagnetic (FM, time-reversal breaking) long-range correlations along the $\hat{a}$ axis as established by magnetization measurements and confirmed by our calculations. States near the Fermi level are dominated by the $j = \frac{5}{2}$ configuration, with the $j_z = \pm\frac{1}{2}$ sectors being effectively degenerate and half-filled. Unlike the small-gap insulating nonmagnetic electronic spectrum, the FM Fermi surfaces are large (strongly metallic) and display low-dimensional features, reminiscent of the FM superconductor UGe$_2$.

I. INTRODUCTION

Crystal symmetries have played a crucial role in classification of superconducting gaps, with the well-studied options being nodeless, point node, or line node gaps. These classes have different types of low-energy excitations, as observed in spectroscopic, thermodynamic, and transport properties. Symmetries also play a central role in the topological classification of normal crystalline materials, leading to topological versus "trivial" insulators, Weyl semimetals, and multi-Weyl semimetals, as well as some more esoteric classes. A conjunction of these criteria was discovered by Agterberg, Brydon, and Timm (ABT) [1], who established the possibility of a superconducting phase with topological protection that retains an *area* of gapless excitations, called by them a Bogoliubov Fermi surface (BFS). The BFS phase combines a conventionally gapped region of a Fermi surface (FS) with an ungapped portion—a normal electronic Fermi surface—resulting in a new phase of matter which for now is called the BFS phase.

This theoretical development is especially prescient because of recent indications of superconducting phases in which a finite fraction of carriers remain ungapped at temperature $T = 0$. A definitive indication is a nonzero Sommerfeld specific heat coefficient well below the superconducting critical temperature T_c, when the sample is sufficiently free of second phases. One example is the Fe(S,Se) alloy system [2,3], and other possible examples have been mentioned by ABT [1]. The basic need at this time is to obtain a realistic band structure including the requisite aspects that will form the platform for inclusion of additional (viz. dynamic) effects.

We focus on the newly synthesized actinide chalcogenide UTe$_2$ that displays unconventional superconductivity.

UTe$_2$, which crystallizes in an orthorhombic *Immm* structure [4] (space group No. 71) shown in Fig. 1, had originally been suggested by Ran and collaborators [5] to provide a new phase of superconducting matter below $T_c = 1.7$ K in which half of the electrons become superconducting and half remain normal (thus with Fermi surfaces), based on heat capacity (C_v) data down to 1.5 K. This result was confirmed by Aoki *et al.* [6], who extended the characterization of UTe$_2$ [7–9]. One scenario was that, at T_c, some additional symmetry is broken beyond the usual broken gauge symmetry that produced a new and unusual state of matter in that *area* of gap nodes, very different from the known possibilities of point and line nodes.

In more recent studies down to 50 mK, Ran *et al.* [5,10] have reported an upturn in C_v/T below 0.5 K, likely involving very low-energy quasilocalized modes (of unknown origin). When this contribution to the entropy is accounted for, the remaining electronic C_v is representative of a point superconducting gap, and strong evidence has been presented for *p*-wave triplet pairing with point nodes. That this behavior occurs in a U-based compound brings to mind the three U-based ferromagnetic superconductors UGe$_2$, URhGe, and UCoGe, with the difference that no magnetic order has been observed in UTe$_2$ down to 25 mK [11]. For a recent review and comparison of the earlier three compounds, see Aoki, Ishida, and Flouquet [12].

Several features of UTe$_2$ have been revealed. The susceptibility is highly anisotropic, being much higher (as temperature is lowered) along the $\hat{a}$ axis. This anisotropy indicates that ferromagnetic ordering is more highly favored along this axis, though ordering does not actually occur in zero magnetic field. This anisotropy implies in turn a strong crystal field

*pickett@physics.ucdavis.edu

anisotropy of the U atom, from which any magnetic moment must arise. UTe$_2$ remains metallic with a large (enhanced) Sommerfeld coefficient of $\gamma \approx 120$ mJ/K^2 [5,6], indicative of a Kondo lattice fermionic ground state. Without any electronic structure study for comparison, the degree of enhancement remains an open question. Aoki *et al.* [6] have reported a 10% entropy imbalance at T_c between the observed state and the extrapolated normal state, which may indicate some more complex behavior below T_c.

While U metallic $5f$ electrons become highly conducting at low T, the magnetic susceptibility at higher temperature (above 150 K) is characteristic of a local Curie-Weiss moment, reported variously as somewhat anisotropic with values in the 3.3–3.6μ_B/U range [4], or also as 2.8μ_B/U [5]. This local-itinerant dichotomy is itself not so unusual, as elemental Fe itself and several heavy fermion materials behave similarly. What is different about U is that the spin-orbit coupling is very large, so pure spin differentiation gives way to spin-orbit coupled quantum designations with the orbital contribution being larger than that of the spin.

The structure of UTe$_2$ is characterized by a shortest U-U distance of 3.78 Å along a "chain" in the a direction, with the next distance being 4.16 Å. This separation is well above the Hill limit [13] of 3.4–3.6 Å for uranium, implying that the $5f$ electrons (or the most tightly bound ones) should be localized and magnetic. The two U sites in the cell are related by inversion. As mentioned, strong magnetic anisotropy in $\chi_{\alpha\alpha}(T)$ establishes $\hat{a}$ as the easy axis, but this raises the question of why no magnetic order down was detected down to 2 K.

Calculations indicate that ferromagnetic (FM) order is strongly favored over antiferromagnetic ordering, when spins are aligned along the $\hat{a}$ direction. The magnetocrystalline anisotropy (MCA) is very large, nearly 100 meV, indicating that indeed FM alignment along $\hat{a}$ is favored and order must be being avoided by fluctuations. The large MCA indicates that crystal fields on the U site should be scrutinized.

We find, as expected, that U $5f$ states dominate the region around the Fermi level, described in Sec. III. Inclusion of correlation effects appropriate for a more localized description versus a fully itinerant description, by including a repulsive Hubbard U interaction and a Hund's J parameter, do not change the primary features but do lead to an effective degeneracy that may be relevant. The states at and below E_F are dominated by $j = \frac{5}{2}$ character (spin opposite to the orbital moment). Within this multiplet, $m_j = -\frac{5}{2}$ and $-\frac{3}{2}$ states, while not quite fully occupied in our density functional theory plus Hubbard U (DFT+U) treatment, likely will become fully occupied and narrower in bandwidth when dynamical effects are included, such as is done in dynamical mean field theory. The $m_j = \pm\frac{1}{2}$ states provide the primary component of Fermi level states, and they are effectively degenerate and half-filled. These projections are with respect to the $\hat{a}$ axis, chosen as the majority spin direction in our work. Furthermore, decomposition into spin states reveals that states around E_F are essentially fully spin-polarized. These characteristics, and the very low-temperature entropy, are suggestive of some incipient broken symmetry and related quantum fluctuations. In Sec. IV some related analysis is provided, and a brief summary is provided in Sec. V.

II. METHODS

The electronic structure has been investigated with the local spin density approximation + Hubbard U (LSDA+U) method reviewed and analyzed in Ref. [14]. Fully anisotropic repulsive orbital interactions $U_{m,m'}$ are included between all U orbitals m, with Hund's coupling $J_{m,m'}$ between parallel spin electrons, both treated in a fully rotationally invariant manner [15]. In the case of strong spin-orbit coupling (SOC) appropriate for U, to treat the strong orbital character realistically the spherical average interaction

$$\Delta E_{SS}^{ee} = \tfrac{1}{2}(\bar{U} - \bar{J})(\mathrm{Tr}[\hat{n}] - \mathrm{Tr}[\hat{n}\hat{n}]) \tag{1}$$

is considered as discussed in Ref. [16]. Here $\hat{n}$ is the orbital occupation matrix of the open shell and $\bar{U}$ and $\bar{J}$ are spherically averaged interactions. The remaining spin and orbitally dependent LSDA+U terms include the SOC induced anisotropic contributions to the on-site Coulomb interactions—the orbital polarization (OP)—and the spin-flip terms due to spin off-diagonal matrix elements of the on-site occupation matrix $\hat{n}_{j_z, j'_z}$.

We use the relativistic version of the full-potential linearized augmented plane wave method including SOC, with the rotationally invariant form of DFT+U implemented as described in Refs. [15,17]. An additional nonspherical double-counting correction is used, described in Refs. [17,18]. Following a conventional approach, we make use of reduced atomic Hartree-Fock values [19] of the Slater integrals $F_2 = 6.20$ eV, $F_4 = 4.03$ eV, and $F_6 = 2.94$ eV. The resulting values are Hund's $J = 0.51$ eV, and we select a Hubbard U (=F_0) equal to the value of J. With the choice of the Coulomb repulsion U equal to the Hund's exchange J, all spherically symmetric terms in the rotationally invariant U and J corrections are set to zero, as they are treated in the LSDA functional. This approach can be regarded as the OP limit of LSDA+U; orbital polarization functionals with DFT [20,21] might also be tried. For complete clarity, the functional we use [22] is presented in detail in Appendix A.

III. ANALYSIS OF RESULTS

A. Nonmagnetic local density approximation (LDA) + U(OP)

As a reference point we first perform nonmagnetic LSDA+U(OP) calculations. The electronic density of states (DOS), together with the U atom f-projected DOS and Te p-projected DOS, is shown in Fig. 1. The $\frac{5}{2}$ and $\frac{7}{2}$ peak centers are separated by ~1 eV. The $\xi \vec{s} \cdot \vec{\ell}$ term in the Kohn-Sham equation has a coefficient of $\xi_{5f} = 220$ meV, giving a $\frac{5}{2}$-$\frac{7}{2}$ splitting of order 0.77 eV, confirming that this separation is from SOC, with minor crystal field contributions. The calculated $5f$ occupation within the U sphere is $n_f = 2.8$, which supports the viewpoint of an underlying f^3 configuration (tails of $5f$ orbitals extend beyond the atomic sphere used in obtaining the 2.8 value). Additional evidence for this is presented later. A filled Te p shell, i.e., Te^{2-}, would require U^{4+} f^2, so the Te p shell is not filled and, despite the small U $5f$ bandwidth, U-Te hybridization cannot be discounted.

The narrow $5f$ electron states shown in Fig. 1 that straddle the Fermi energy ($E_F = 0$) have $j = \frac{5}{2}$ character; the $j = \frac{7}{2}$ manifold is centered 1.5 eV above E_F. Careful determination
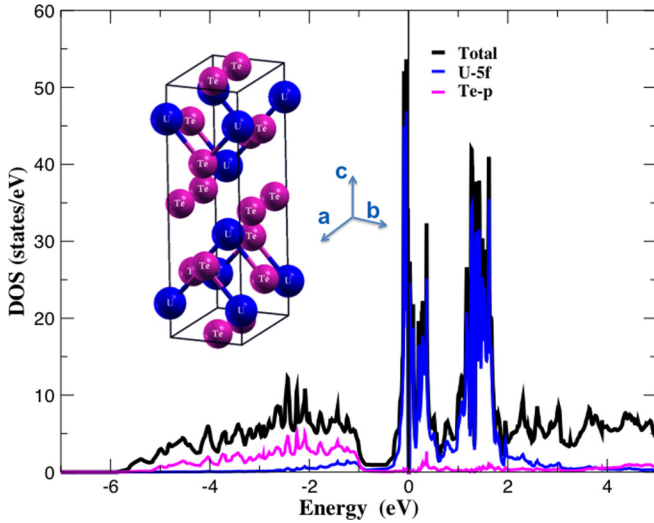
FIG. 1. Total and projected densities of states/eV (per unit cell) for nonmagnetic UTe$_2$ from the local spin density approximation plus Hubbard U [LSDA $+ U$(OP)] functional, showing the total (black) and projections for U $5f$ (blue) and Te $5p$ (magenta). The *Immm* UTe$_2$ crystal structure is shown in the inset: blue spheres are U, and magenta spheres are Te. Note that the states near the Fermi level $E_F = 0$ are entirely U $5f$ in character.

of the bands and DOS reveals a gap of 13 meV, apparently an "accidental" hybridization gap rather than one between characteristic bands (bonding-antibonding, specific m_j characters, etc.) Due to a flatness of the f bands there is a strong peak in the DOS (up to 35 states/eV) just 15 meV below E_F which would correspond to $\gamma = 41$ mJ K^{-2} mol^{-1}. Even that value is much smaller than the experimental value of $\gamma = 120$ mJ K^{-2} mol^{-1} [5], indicating a substantial dynamical enhancement which, considering the Kondo-like behavior observed in the resistivity, is likely due to magnetic fluctuations.

An enlargement of the band structure near E_F is shown in Fig. 2. Simple nonmagnetic, uncorrelated UTe$_2$ is calculated to be a semimetal, similar to that found by Aoki *et al.* [6] using LDA without correlation corrections. The 13-meV band gap just above E_F reflects a hybridization gap occurring between a heavy band and a light band, although the band structure is more involved than the textbook viewpoint. The semimetallic character of nonmagnetic UTe$_2$ might suggest an instability toward electron-hole pairing [24], though there is no evidence of such a new phase. Also, we find in the next section that OP changes the Fermi level electronic structure substantially.

The $|m_l, m_s\rangle$ and $|m_j = m_l + m_s\rangle$ decompositions of $N(E_F)$ are provided in Table I of Appendix B. Since the experimental susceptibility is highly anisotropic at low T, being much higher along the $\hat{a}$ axis, we chose it as the moment quantization axis and it is used below in the results for ferromagnetic alignment. The major contribution to the FS comes from $m_l = 0$ and $m_s = -\frac{1}{2}$ and from $m_l = -1$ and $m_s = +\frac{1}{2}$ in equal amounts, providing the orbital and spin composition of the active orbitals. Given the strong SOC of U, the angular momentum coupled representation is more fundamental. The decomposition $|j = \frac{5}{2}, m_j = \pm\frac{1}{2}\rangle$ states (henceforward, this notation will be $|\frac{5}{2}, \pm\frac{1}{2}\rangle$) plus some non-negligible amount of $|\frac{5}{2}, \pm\frac{5}{2}\rangle$ states are dominant.
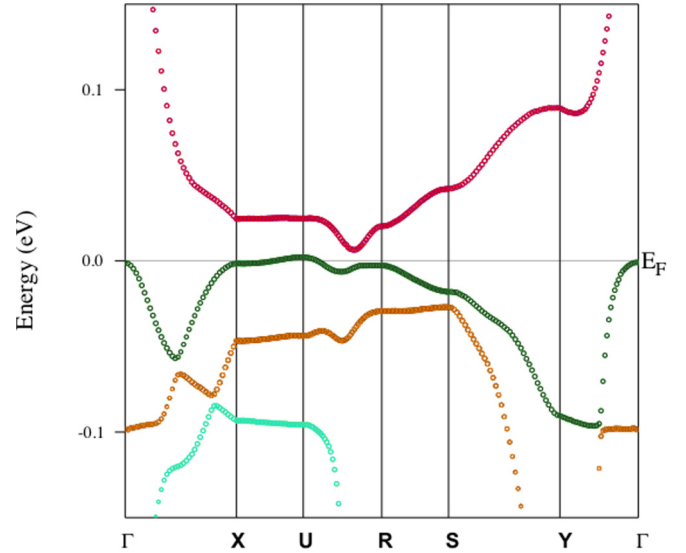

FIG. 2. The band structure from nonmagnetic LSDA$+U$(OP) calculations, which is essentially unchanged from the LSDA bands (the high-symmetry k points $\Gamma[0, 0, 0]$, $X[\pi/a, 0, 0]$, $U[\pi/a, 0, \pi/c]$, $R[\pi/a, \pi/b, \pi/c]$, $S[\pi/a, \pi/b, 0]$, $Y[0, \pi/b, 0]$ [23] were used). Without magnetism there is a 13-meV gap. The colors simply distinguish the bands. The circle size, which indicates the amount of f character of the eigenstates, is uniform in this region because the states are uniformly and almost totally U $5f$ in character, consistent with Fig. 1.

In Appendix C information on the composition of the bands near E_F is provided. The "fat-band" structure is displayed there, emphasizing the $|m_l, m_s\rangle$ and $|m_j = m_l + m_s\rangle$ character of the $j = \frac{5}{2}$ manifold, for negative m_j.

B. Ferromagnetic LSDA+U(OP)

No magnetic order has been detected down to 0.4 K. However, based on the observed susceptibility and strong MCA from both theory and experiment, slow long-range FM correlations with alignment along the $\hat{a}$ axis are expected; i.e., locally the electronic structure can be treated as FM. To model this low-T phase we have performed FM calculations with spin moments (and in this collinear calculation, the orbital moments as well) aligned along the $\hat{a}$ axis. The FM state is 185 meV/f.u. lower in the energy than the nonmagnetic state. The f-shell ordered moments, oriented along the $\hat{a}$ axis, are calculated to be

$\vec{M} \parallel \hat{a}$: $M_S = 1.92\mu_B$, $M_L = -3.44\mu_B$, $M_J = -1.52\mu_B$,
$\vec{M} \parallel \hat{b}$: $M_S = 1.83\mu_B$, $M_L = -3.71\mu_B$, $M_J = -1.88\mu_B$,
$\vec{M} \parallel \hat{c}$: $M_S = 1.91\mu_B$, $M_L = -3.97\mu_B$, $M_J = -2.06\mu_B$.

An analogous calculation for FM UGe$_2$ gave $M_S = 1.32\mu_B$, $M_L = -2.92\mu_B$, and $M_J = -1.58\mu_B$, which was in good agreement with experimental data [25] in the ordered state.

The Curie-Weiss moment, an average over fluctuations in all dimensions, is $2.8\mu_B$ [5] to $3.3\mu_B$ [6] for UTe$_2$. It is common, when moments are not strongly localized, that the ordered moment is reduced due to mixing with the conduction states. Lack of ordering in UTe$_2$ precludes comparison, but substantial itinerant character of the moment is apparent.
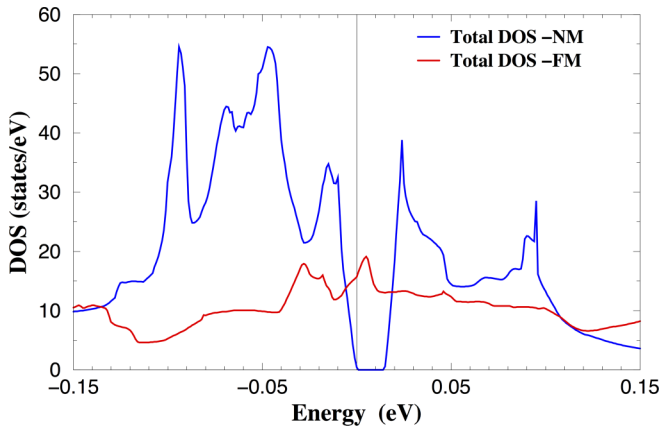
FIG. 3. Comparison of the density of states for ferromagnetic alignment (metallic) with that of the gapped nonmagnetic state, on a fine energy scale. The 13-meV gap is thoroughly washed out when magnetic moments are allowed to emerge and align.

Calculating the magnetocrystalline anisotropy, we find that for moments oriented along the $\hat{b}$ and $\hat{c}$ axes, the energy is higher by 37 and 96 meV/f.u. respectively. Thus, there is a strong uniaxial magnetic anisotropy, with $\hat{a}$ being the easy axis.

The effect of allowing FM moment development and alignment is displayed in Fig. 3. The strong spin- and orbital-polarization coupled with strong SOC results in washing out of the small hybridization gap calculated for the nonmagnetic system. The value of $N(E_F)$ is 16 states/eV-cell corresponding to a band value of $\gamma_\circ = 19$ mJ/K^2, leaving a factor of 6 enhancement due to dynamic processes to account for the observed Sommerfeld coefficient.

The density of states for FM ordered UTe$_2$, projected onto spin directions, is displayed in Fig. 4(a). The exchange splitting is seen to be around 1.5 eV, with negligible population of minority spin 5f orbitals—the f shell of U is effectively spin-polarized, however SOC mixes the spin moment amongst the m_j states. The U j_z-projected DOS for both $j = \frac{5}{2}$ and $j = \frac{7}{2}$ subspaces is pictured in Fig. 4(b). The $j = \frac{5}{2}$ states with $j_z = -\frac{5}{2}$ and $-\frac{3}{2}$ are so nearly filled that they should be considered as localized, with negligible amplitude of excitation at low temperature. The $j_z = \pm\frac{1}{2}$ states are half-filled, a point we return to below; higher j_z states are unfilled. The U atom configuration can thus be characterized as an f^2 local moment, with $j_z = \pm\frac{1}{2}$ orbitals that are itinerant and whose spin whose spin components of equal magnitudes lie in opposite directions and thus contribute nothing to the net spin moment.

The Fermi surface for FM order is displayed in Fig. 5. It has four sheets, with the most obvious characteristic being a strong nesting feature for FS-3 near $(0, \frac{\pi}{b}, 0)$. Such nearly parallel sheets, such as would arise from a one-dimensional band, suggest instabilities toward order that would double the cell along the $\hat{b}$ axis. The $|m_j = m_l + m_s\rangle$ decompositions of $N(E_F)$ are given in Table II of Appendix B. The corresponding $|m_l, m_s\rangle$ decompositions of $N(E_F)$ are provided in Appendix B in Table III. From Table II, it can be observed that FS-2 has strong $j_z = \frac{1}{2}$ character while FS-4 has strong $j_z = -\frac{1}{2}$ character, with some $j_z = \pm\frac{1}{2}$ character spread over the other sheets.
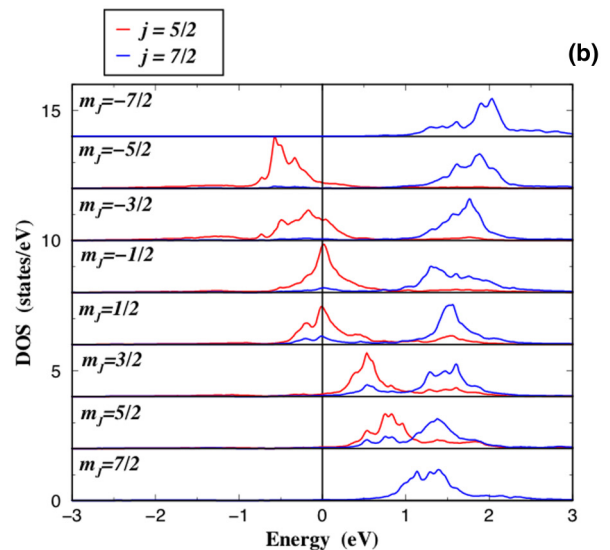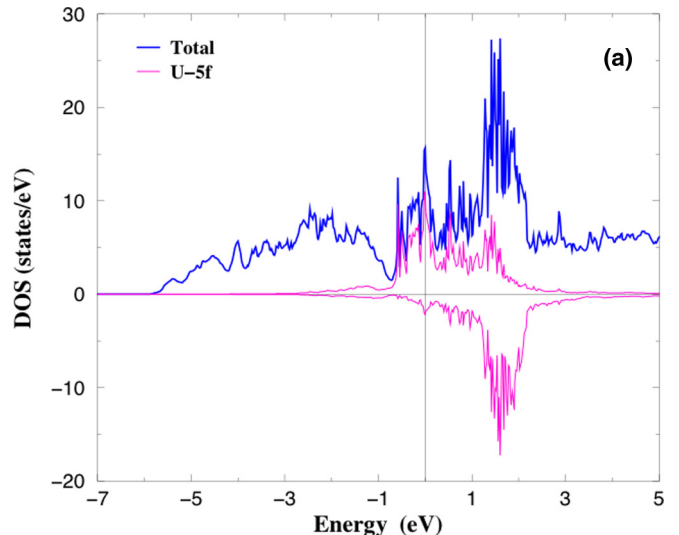

FIG. 4. Total (a) and f-projected (b) densities of states for ferromagnetic UTe$_2$ from LSDA+U(OP) functional, with the moment along the easy $\hat{a}$ axis. In panel (a) the majority spin 5f states are plotted upward and the minority spin states are plotted downward, both in red. In panel (b) the j_z-decomposed DOS for both $j = \frac{5}{2}$, plotted in red, and $j = \frac{7}{2}$, shown in blue, are displayed. Occupied states arise almost entirely from $j = \frac{5}{2}$ states with negative j_z. Note the orderly progression in energy of both $\frac{5}{2}$ and $\frac{7}{2}$ manifolds.

IV. CONSIDERATIONS FOR PARTIAL PAIRING

We have suggested that at low T near T_c, the long-range and slow magnetic fluctuations imply that UTe$_2$ can be treated as locally FM. In this case spin degeneracy is broken, and moreover strong SOC mixes the two spins with orbital characters. The bands and Fermi surfaces are nondegenerate, but inversion provides $\varepsilon_{-k} = \varepsilon_k$ as the only degeneracy. Averaging over the moment fluctuations restores moment symmetry on a timescale slower than that of the fluctuation time. The next consideration is that the resistivity indicates that Kondo coherence has restored a translationally invariant state ("screened the moments") that does not scatter carriers.
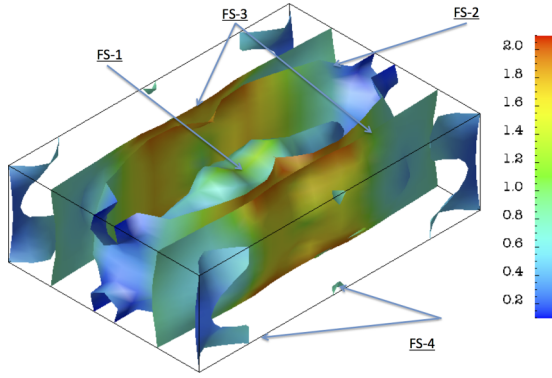
FIG. 5. Fermi surface for FM order, from LSDA+U(OP), centered at the Γ point. The Fermi surface is large and multisheeted, with a nesting feature for FS-3 near $(0, \frac{\pi}{b}, 0)$. FS-1 is in the center; FS-2 parallels FS-3 along parts of its length. The low velocities, given by the colorbar, extend over at least an order of magnitude, up to nearly 2 eV/Å ($\sim 2.5 \times 10^7$ cm/s).

This coherence and lack of broken symmetry suggests that degeneracy, viz. up-down, is restored. On the other hand, the large susceptibility implies that fluctuations of large moments remain present.

A. Local spin-orbital considerations

The effective degeneracy of the $m_j = \pm\frac{1}{2}$ orbitals and their half-filling suggests possible incipient instabilities involving some linear combinations of the degenerate orbitals, which are themselves linear combinations of $5f$ orbitals and spin projections. The spin-orbit coupled combinations of $m_j = \pm\frac{1}{2}$ states are [26]

$$\phi_{\frac{5}{2},+\frac{1}{2}} = -\sqrt{\frac{3}{7}}Y_{3,0}|\uparrow\rangle + \sqrt{\frac{4}{7}}Y_{3,+1}|\downarrow\rangle,$$

$$\phi_{\frac{5}{2},-\frac{1}{2}} = -\sqrt{\frac{3}{7}}Y_{3,-1}|\uparrow\rangle + \sqrt{\frac{4}{7}}Y_{3,0}|\downarrow\rangle, \quad (2)$$

in terms of spherical harmonics $Y_{\ell,m}$ and spin projections. Each state contains $Y_{3,0}$ but with opposite spin projections and somewhat different weights. Rotating these degenerate orbitals in functional space so the common orbital $Y_{3,0}$ has equal spin-up and -down amplitudes leads to the combinations

$$\Phi_\pm = \left[\sqrt{\frac{4}{7}}\phi_{\frac{5}{2},+\frac{1}{2}} \pm \beta\sqrt{\frac{3}{7}}\phi_{\frac{5}{2},-\frac{1}{2}} \right]$$

$$= \left[\sqrt{\frac{16}{49}}Y_{3,+1}|\downarrow\rangle \mp \beta\sqrt{\frac{9}{49}}Y_{3,-1}|\uparrow\rangle \right]$$

$$+ \sqrt{\frac{24}{49}}Y_{3,0}\frac{[-|\uparrow\rangle \pm \beta|\downarrow\rangle]}{\sqrt{2}}, \quad (3)$$

where $\beta = 1$ or $\beta = i$. This rotation leads to the orbital function $Y_{3,0}$ with vanishing orbital moment and a specific spin projection: $\langle \vec{s} \rangle = (0, \pm 1, 0)$. this component has zero projection along the orbital z axis, which due to the large magnetic anisotropy is the crystalline $\hat{a}$ axis, as well a zero angular moment along $\hat{z}$. The other part has entwined $(Y_{3,\pm 1})$ orbitals with opposite spin projections.

A second intriguing observation is that the $Y_{3,0}$ component has a fraction $\frac{24}{49} = 49\%$ of the weight, while the second contains 51%. These fractions, experimentally indistinguishable from $\frac{1}{2}$, suggest incipient symmetry breaking that links the magnetic anisotropy and spin versus orbital contributions to the moment, providing a possible platform for assessing spin-orbital fluctuations.

B. The coherent-carrier itinerant picture

The Fermi liquid behavior, evidenced by the strong decrease in the resistivity by a factor of up to 35 below 50 K [6], reflects Kondo screening of the $5f$ moments. While the large susceptibility, arising from field alignment of magnetic fluctuations, indicates dynamic moments, they no longer scatter carriers, primarily just contributing a mass enhancement which we can estimate from comparing the specific heat γ with the band value to be of the order of a factor of 6.

Aoki, Ishida, and Floquet have observed in their review [12] that only uranium compounds have been confirmed as FM superconductors: orthorhombic UXGe, $X = $ Ge, Rh, and Co. The latter two are isovalent. We obtain an f^3 configuration in UTe$_2$, just as has been concluded experimentally for UCoGe [12], so the f^3 configuration may carry special significance.

For weak ferromagnets and incipient ferromagnets, DFT methods are known to overestimate the tendency toward magnetic order and the size of magnetic moments, usually ascribed to neglect of magnetic fluctuation effects in the functionals, and possibly to the necessity to include dynamic effects explicitly. Our work provides the groundwork for modeling the metallic Fermi liquid phase of UTe$_2$ that provides the platform for an exotic superconducting state. In UPt$_3$ for example, the six-sheeted Fermi surface is given very realistically by LDA methods [27–31]. In some other cases, however, Fermi surfaces are not predicted well by first-principles methods.

Our work provides important guidelines: the heavy fermion Fermi liquid state of UTe$_2$ is built on an f^3 U configuration in which $m_j = \pm\frac{1}{2}$ states in the $j = \frac{5}{2}$ subspace provides the primary orbital content of the Fermi surface states $|k, n, \tau\rangle$. Here τ indicates the pseudospin component that bears some characteristics of the more common spin degrees of freedom that are commonly used to categorize exotic pairing states. The specific spin-orbital decompositions discussed in the previous subsection may deserve further consideration.

V. DISCUSSION AND SUMMARY

UTe$_2$ presents the usual challenges of a Kondo lattice superconductor, with the complicating features of strong magnetic anisotropy (rising from its strong spin-orbit coupling and low site symmetry. At low T, magnetic fluctuations slow down, especially those with large moments as observed in UTe$_2$. Considering the strong evidence, both experimental and theoretical, of an easy $\hat{a}$ axis and strong magnetocrystalline anisotropy, an outstanding question is how UTe$_2$ manages to avoid magnetic order. Kondo screening of the moments is the primary rationalization.

TABLE I. The $|m_l, m_s\rangle$ and $|j, m_j\rangle$ decompositions of the U atom f-projected DOS at E_F (in states/eV unit cell) for the unpolarized system. The magnetic quantization is along the easy $\hat{a}$ axis.

				m_l				
	−3	−2	−1	0	1	2	3	
Spin-↑	0.16	0.04	0.10	0.16	0.01	0.03	0.00	
Spin-↓	0.00	0.03	0.01	0.16	0.10	0.04	0.16	
				m_j				
	−7/2	−5/2	−3/2	−1/2	1/2	3/2	5/2	7/2
	0	0.19	0.05	0.26	0.26	0.05	0.19	0

Comparison and contrast of UTe$_2$ and UPd$_2$Al$_3$ [32] are striking. Both have comparable specific heat γ's indicating Kondo lattice character arising from spin fluctuations, and both become superconducting at 1.7–1.8 K. Both can be characterized as having a local moment from a localized f^2 pair of orbitals, with roughly one more $5f$ electron being itinerant. However, UPd$_2$Al$_3$ orders antiferromagnetically at a temperature six times higher than T_c, contrasting to UTe$_2$ which (according to muon spin rotation data [33]) does not order magnetically down to 50 mK. Evidently the phases in these intermetallic uranium compounds are sensitive to several relative energy scales.

We have explored the possibility that at low T (somewhat above the superconducting T_c) there is medium-range FM orientation of the U moments, from $j = \frac{5}{2}$ states (quantization axis is the $\hat{a}$ axis) which have strong localized character (moments around 2–3μ_B) but strong enough hopping to enable conducting behavior of the $5f$ carriers with correlation enhancements. In this scenario the U sites are locally ferromagnetic, involving essentially pure spin (majority) moments shared among several $5f$ orbitals. Magnetic (exchange) coupling proceeds through the spin moments, so the single-spin character of the calculated moments becomes relevant. In the limit of negligible SOC and one spin channel being frozen out, triplet pairing reduces to single-spin superconducting pairing [34,35] suggested as a possibility in half-metals.

We have presented a scenario for this division: the Clebsch-Gordon coupling enforced by strong SOC suggests a coupling that favors the choice of spatially uniform, orbital-moment-free, spin-mixed spin orbitals as the building blocks for the Bloch orbitals that will eventually pair. The linear combination that suggests the importance of these orbitals contains 49% of the Fermi level spectral density of $j_z = \pm\frac{1}{2}$ states that are calculated to be effectively degenerate in the correlated band structure of this heavy fermion compound. The half-filled nature of these $j_z = \pm\frac{1}{2}$ orbitals, with the density of states peaking at E_F, suggests the tendency toward symmetry-breaking states.

Recently, other papers or preprints containing electronic structure predictions have appeared. Aoki *et al.* [6] presented a local density approximation (no correlation, no magnetism) band structure possessing a small gap, in agreement with our results for this case. However, our spin-polarized and correlated treatment do not support their proposal of a nearby Kondo insulating phase. Dynamical mean field theory results for the seemingly unrealistically large value of Hubbard $U = 8$ eV have been discussed by Xu *et al.* [36]. Ishizuka and collaborators [37] report DFT+U calculations with a somewhat different functional than we use, but with similar Hubbard $U = 1$ eV, resulting in large Fermi surfaces, somewhat what we have reported here. We anticipate that modest values of U around 1 eV are most reasonable for UTe$_2$, as they allow itinerant description of the uppermost occupied valence band states while adjusting the effectively localized $5f$ states at higher binding energy.

TABLE II. Decomposition of the four Fermi surface contributions to $N(E_F)$ from $|m_j = m_l + m_s\rangle$ projections, for FM aligned UTe$_2$. Magnetic quantization is along the $\hat{a}$ axis. The dominance of the $j_z = \pm\frac{1}{2}$ is evident.

				m_j				
	−7/2	−5/2	−3/2	−1/2	1/2	3/2	5/2	7/2
FS1	0	0.02	0.17	0.15	0.25	0.01	0.03	0.01
FS2	0	0.08	0.21	0.71	1.35	0.06	0.03	0.01
FS3	0	0.05	0.23	0.63	0.36	0.04	0.02	0.01
FS4	0	0.04	0.27	1.30	0.48	0.04	0.02	0.01
Sum	0	0.19	0.88	2.79	2.44	0.15	0.10	0.04

APPENDIX A: THE EXCHANGE-CORRELATION FUNCTIONAL

The electron-electron interaction energy E^{ee} in the DFT+U total-energy functional [22] has the form

$$E^{ee} = \frac{1}{2} \sum_{\gamma_1 \gamma_2 \gamma_3 \gamma_4} n_{\gamma_1 \gamma_2} \left(V^{ee}_{\gamma_1 \gamma_3; \gamma_2 \gamma_4} - V^{ee}_{\gamma_1 \gamma_3; \gamma_4 \gamma_2} \right) n_{\gamma_3 \gamma_4}, \tag{A1}$$

which contains the 14×14 on-site occupation matrix $n_{\gamma_1 \gamma_2} \equiv n_{m_1 \sigma_1, m_2 \sigma_2}$ with generally nonzero orbital and spin off-diagonal matrix elements. The V^{ee} is an effective on-site Coulomb interaction, expressed in terms of Slater integrals (see Eq. (3) in Ref. [15]) which are linked to intra-atomic repulsion $U_{m,m'}$ and exchange $J_{m,m'}$ quantities mentioned in Sec. II. The spherically symmetric double-counting energy E^{dc} is subtracted from E^{ee} to correct the electron-electron interaction already included in DFT.

The DFT+U energy correction $\Delta E^{ee} = E^{ee} - E^{dc}$ can be divided into a sum of spherically symmetric and anisotropic terms. In the case of the "atomic" or "fully localized" limit of E^{dc}, and without SOC, the spherically symmetric part is given by [16]

$$\Delta E^{ee} = \frac{(U - J)}{2} (\text{Tr}[\hat{n}] - \text{Tr}[\hat{n}\hat{n}]). \tag{A2}$$

The choice $U = J$ in Eq. (A1) means that the spherically symmetric part of ΔE^{ee} given by Eq. (A2) becomes equal to zero. The remaining nonspherically symmetric part of ΔE^{ee} can be regarded as the DFT+U analog of the proposed "orbital polarization correction" functionals [20,21].

Due to the full potential character, care should be taken to exclude the so-called "nonspherical double counting" of the f-state nonspherical contributions to the DFT and DFT+U parts of the Kohn-Sham potential. When the atomic sphere matrix elements of the DFT+U Hamiltonian are calculated, those contributions from the lattice harmonics K_ν of the nonspherical part of the DFT potential $V^{\text{NSH}}_{\text{DFT}}(\mathbf{r}) = \sum_\nu V_\nu(r) K_\nu(\hat{r})$ are removed, which are proportional to $\langle lm_1 | K_\nu | lm_2 \rangle$ for $l = 3$, the f-state orbital quantum number.

APPENDIX B: DECOMPOSITION OF THE U 5f DOS AT E_F

Table III indicates the stated decomposition of the Fermi level density of states.

TABLE III. The $|m_l, m_s\rangle$ decomposition of $N_f(E_F)$ (eV^{-1}), for ferromagnetic alignment of UTe$_2$ along the $\hat{a}$ axis. The spin-down components are small; as noted in the text, the system is near full spin polarization.

				m_l			
	-3	-2	-1	0	1	2	3
				FS1			
Spin-↑	0.02	0.14	0.10	0.20	0.01	0.02	0.01
Spin-↓	0.00	0.00	0.03	0.05	0.05	0.00	0.01
				FS2			
Spin-↑	0.08	0.18	0.60	1.12	0.04	0.02	0.01
Spin-↓	0.00	0.00	0.03	0.11	0.23	0.02	0.01
				FS3			
Spin-↑	0.05	0.20	0.52	0.30	0.02	0.02	0.01
Spin-↓	0.00	0.00	0.03	0.11	0.06	0.02	0.01
				FS4			
Spin-↑	0.04	0.24	1.07	0.40	0.01	0.01	0.01
Spin-↓	0.00	0.00	0.03	0.23	0.08	0.01	0.01

APPENDIX C: 5f ORBITAL CONTRIBUTION NEAR E_F

Figure 6 provides the relative amounts of the stated spin-orbital characters of states near the Fermi level. The bands on the zone boundary X-U-R-S are flatter. More dispersion occurs along Γ-X and S-Y.
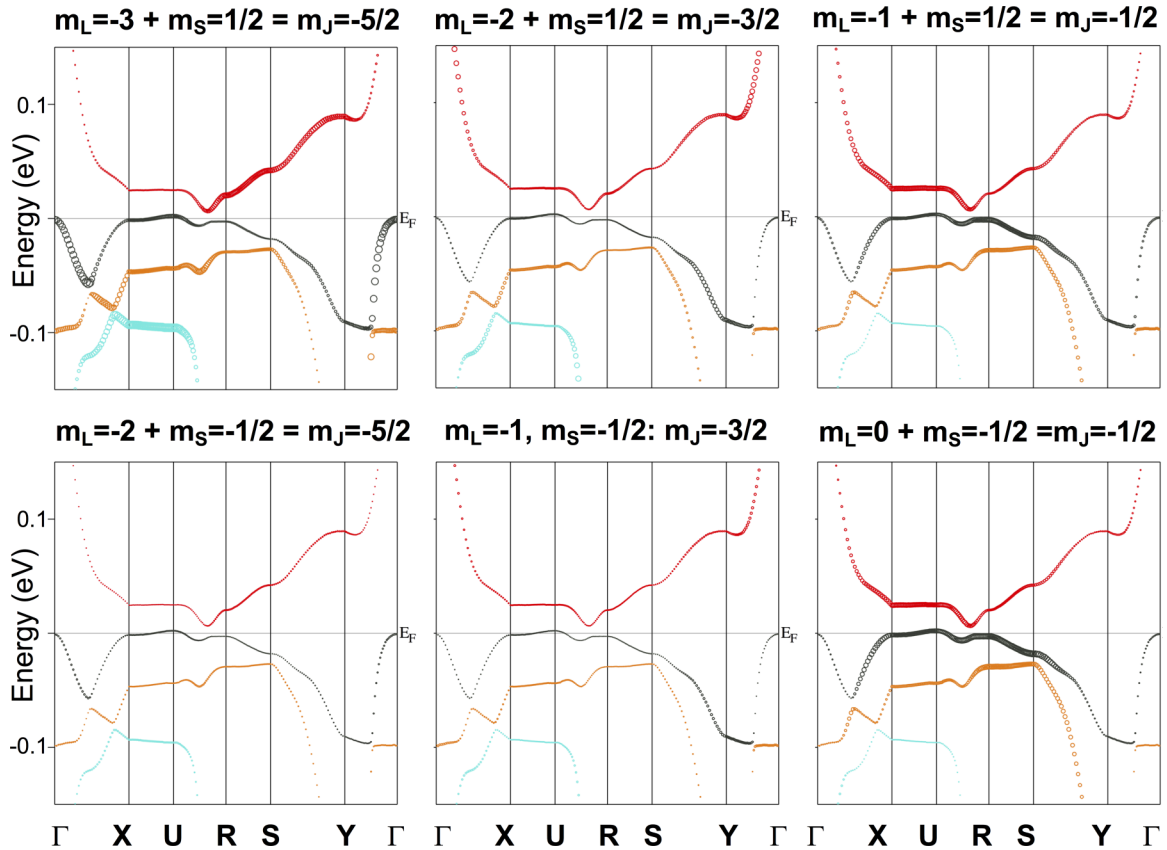

FIG. 6. The 5f fat-band structure of nonmagnetic UTe$_2$ from LDA+U(OP) calculations. The circle size indicates the amount of $j = \frac{5}{2}$ and m_j character in the bands, as indicated. The two contributions to the $j_z = -\frac{5}{2}$ character are quite different; the differences in the other two cases isare not so pronounced. Note that the full energy range is only 300 meV.

[1] D. F. Agterberg, P. M. R. Brydon, and C. Timm, Bogoliubov Fermi Surfaces in Superconductors with Broken Time-Reversal Symmetry, Phys. Rev. Lett. **118**, 127001 (2017).

[2] Y. Sato, S. Kasahara, T. Taniguchi, X. Xing, Y. Kasahara, Y. Tokiwa, Y. Yamakawa, H. Kontani, T. Shibauchi, and Y. Matsuda, Abrupt change of the superconducting gap structure at the nematic critical point in FeSe$_{1x}$S$_x$, Proc. Natl. Acad. Sci. USA **115**, 1227 (2018).

[3] C. Setty, S. Bhattacharyya, A. Kreisel, and P. Hirschfeld, Ultranodal pair states in iron-based superconductors, arXiv:1903.00481.

[4] S. Ikeda, H. Sakai, D. Aoki, Y. Homma, E. Yamamoto, A. Nakamura, Y. Shiokawa, Y. Haga, and Y. Onuki, Single crystal growth and magnetic properties of UTe$_2$, J. Phys. Soc. Japan **75** (Suppl.), 116 (2006).

[5] S. Ran, C. Eckberg, Q.-P. Ding, Y. Furukawa, T. Metz, S. R. Saha, I.-L. Liu, M. Zic, H. Kim, J. Paglione, and N. P. Butch, Spontaneously polarized half-gapped superconductivity, Science **365**, 684 (2019).

[6] D. Aoki, A. Nakamura, F. Honda, D. Li, Y. Homma, Y. Shimizu, Y. J. Sato, G. Knebel, J.-P. Brison, A. Pourret, D. Braithwaite, G. Lapertot, Q. Niu, M. Valiska, H. Harima, and J. Flouquet, Unconventional superconductivity in heavy fermion UTe$_2$, J. Phys. Soc. Jpn. **88**, 043702 (2019).

[7] A. Miyake, Y. Shimizu, Y. J. Sato, D. Li, A. Nakamura, Y. Homma, F. Honda, J. Flouquet, M. Tokunaga, and D. Aoki, Metamagnetic transition in heavy fermion superconductor UTe$_2$, J. Phys. Soc. Jpn. **88**, 063706 (2019).

[8] G. Knebel, W. Knafo, A. Pourret, Q. Niu, M. Vališka, D. Braithwaite, G. Lapertot, M. Nardone, A. Zitouni, S. Mishra, I. Sheikin, G. Seyfarht, J.-P. Brison, D. Aoki, and J. Flouquet, Field-reentrant superconductivity close to a metamagnetic transition in the heavy-fermion superconductor UTe$_2$, J. Phys. Soc. Jpn. **88**, 063707 (2019).

[9] Q. Niu, G. Knebel, D. Braithwaite, D. Aoki, G. Lapertot, G. Seyfarth, J.-P. Brison, J. Flouquet, and A. Pourret, Fermi-surface instabilities in the heavy-fermion superconductor UTe$_2$, arXiv:1907.11118.

[10] T. Metz, S. Bae, S. Ran, I.-L. Liu, Y. S. Eo, W. T. Fuhrman, D. F. Agterberg, S. Anlage, N. P. Butch, and J. Paglionnne, Point node gap structure of spin-triplet superconductor UTe$_2$, arXiv:1908.01069.

[11] S. Sundar, S. Gheidi, K. Akintola, A. M. Cote, S. R. Dunsiger, S. Ran, N. P. Butch, S. R. Saha, J. Paglione, and J. E. Sonier, Coexistence of ferromagnetic fluctuations and superconductivity in the actinide superconductor UTe$_2$, arXiv:1905.06901.

[12] D. Aoki, K. Ishida, and J. Floquet, Review of U-based ferromagnetic superconductors: Comparison between UGe2, URhGe, and UCoGe, J. Phys. Soc. Jpn. **88**, 022001 (2019).

[13] H. Hill, in *Plutonium 1970*, edited by W. N. Miner (AIME, New York, 1970), pp. 2–19.

[14] E. R. Ylvisaker, K. Koepernik, and W. E. Pickett, Anisotropy and magnetism in the LSDA+U Method, Phys. Rev. B **79**, 035103 (2009).

[15] A. B. Shick, A. I. Liechtenstein, and W. E. Pickett, Implementation of the LDA+U method using the full-potential linearized augmented plane-wave basis, Phys. Rev. B **60**, 10763 (1999).

[16] S. L. Dudarev, G. A. Botton, S. Y. Savrasov, C. J. Humphreys, and A. P. Sutton, Electron-energy-loss spectra and the structural stability of nickel oxide: An LSDA+U study, Phys. Rev. B **57**, 1505 (1998).

[17] A. B. Shick, V. Janis, V. Drchal, and W. E. Pickett, Spin and orbital magnetic state of UGe$_2$ under pressure, Phys. Rev. B **70**, 134506 (2004).

[18] O. Kristanovski, A. B. Shick, F. Lechermann, and A. I. Lichtenstein, Role of nonspherical double counting in DFT+DMFT: Total energy and structural optimization of pnictide superconductors, Phys. Rev. B **97**, 201116(R) (2018).

[19] K. T. Moore and G. van der Laan, Nature of the $5f$ states in actinide metals, Rev. Mod. Phys. **81**, 235 (2009).

[20] O. Eriksson, M. S. S. Brooks, and B. Johansson, Orbital polarization in narrow-band systems: Application to volume collapses in light lanthanides, Phys. Rev. B **41**, 7311 (1990).

[21] H. Eschrig, M. Sargolzaei, K. Koepernik, and M. Richter, Orbital polarization in the Kohn-Sham-Dirac theory, Europhys. Lett. **72**, 611 (2005).

[22] I. V. Solovyev, A. I. Liechtenstein, and K. Terakura, Is Hund's Second Rule Responsible for the Orbital Magnetism in Solids?, Phys. Rev. Lett. **80**, 5758 (1998).

[23] C. J. Bradley and A. P. Cracknell, *The Mathematical Theory of Symmetry in Solids* (Clarendon, Oxford, 1972), p. 758.

[24] B. A. Volkov, Y. V. Kopaev, and A. I. Rusinov, Theory of excitonic ferromagnetism, JETP **68**, 1899 (1975).

[25] N. Kernavanois, B. Grenier, A. Huxley, E. Ressouche, J.-P. Sanchez, and J. Flouquet, Neutron scattering study of the ferromagnetic superconductor UGe$_2$, Phys. Rev. B **64**, 174509 (2001).

[26] L. D. Landau and I. M. Lifshitz, *Quantum Mechanics: Non-relativistic Theory* (Pergamon, Oxford, 1958), p. 408.

[27] C. S. Wang, H. Krakauer, and W. E. Pickett, Electronic structure and mass enhancement of the heavy fermion superconductor UPt$_3$, Physica B+C **135**, 34 (1985).

[28] C. S. Wang, H. Krakauer, and W. E. Pickett, Unconventional superconductivity and normal-state properties in the heavy fermion superconductor UPt$_3$, J. Phys. F **16**, L287 (1986).

[29] M. R. Norman, R. C. Albers, A. M. Boring, and N. E. Christensen, Fermi surface and effective masses for the heavy-electron superconductor UPt$_3$, Solid State Commun. **68**, 245 (1988).

[30] C. S. Wang, M. R. Norman, R. C. Albers, A. M. Boring, W. E. Pickett, H. Krakauer, and N. E. Christensen, Fermi surface of UPt$_3$ within the local-density approximation, Phys. Rev. B **35**, 7260 (1987).

[31] G. J. McMullan, P. M. C. Rourke, M. R. Norman, A. D. Huxley, N. Doiron-Leyraud, J. Flouquet, G. G. Lonzarich, A. McCollam, and S. R. Julian, The Fermi surface and f-valence electron count of UPt$_3$, New J. Phys. **10**, 053029 (2008).

[32] Y. Tokunaga *et al.*, ^{125}Te-NMR study on a single crystal of heavy fermion superconductor UTe$_2$, J. Phys. Soc. Jpn. **88**, 073701 (2019).

[33] S. Sudar *et al.*, Coexistence of ferromagnetic fluctuations and superconductivity in the actinide superconductor UTe$_2$, arXiv:1905.06901.

[34] W. E. Pickett, Single Spin Superconductivity, Phys. Rev. Lett. **77**, 3185 (1996).

[35] R. E. Rudd and W. E. Pickett, Single spin superconductivity: Formulation and Ginzburg-Landau theory, Phys. Rev. B **57**, 557 (1998).

[36] Y. Xu, Y. Shend, and Y.-F. Yang, Quasi-two-dimensional Fermi surfaces and unitary spin-triplet pairing in the heavy fermion superconductor UTe$_2$, arXiv:1908.07396.

[37] J. Ishizuka, S. Sumita, A. Daido, and Y. Yanase, Insulator-metal transition and topological superconductivity in UTe$_2$ from a first-principles calculation, arXiv:1908.04004.